Pol-InSAR and Pol-TomSAR

Carlos López-Martínez, Eric Pottier

1 Polarimetric SAR Interferometry (Pol-InSAR) 2
1.1 Introduction 2
1.2 SAR Interferometry 2
1.3 Algorithms for Optimum Interferogram Generation 5
1.4 Model Based Polarimetric SAR Interferometry 7
1.4.1 PolInSAR for Bare Surface Scattering 7
1.4.2 Pol-InSAR for Random Volume Scattering 7
1.4.3 PolInSAR 2-Layer Combined Surface and Random Volume Scattering 9
2 Polarimetric SAR Tomography (Pol-TomSAR) 11
2.1 Introduction 11
2.2 SARtom and Pol-TomSAR as Spectral Estimation Problems 12
2.2.1 Non-model Based Adaptive Solutions 12
2.2.2 Model-based Pol-TomSAR 14
2.3 Coherence Tomography 14

1 Polarimetric SAR Interferometry (Pol-InSAR)

1.1 Introduction

This section is devoted to the radar remote sensing technique called polarimetric interferometry [R94][R95][R96][R97]. When used with imaging synthetic aperture radar (SAR) system, it is usually termed Polarimetric Interferometric SAR or PolInSAR for short [R98]. POLInSAR has important applications in the remote measurement of vegetation properties such as forest height [R99] and biomass [R100] and developing future applications in [R101][R102], snow/ice thickness monitoring [R103][R104] and urban height and structure applications [R105]. As its name suggests, this technique combines two separate radar technologies, polarimetry and interferometry. The former, as detailed in the previous sections, involves switching the polarisation state of transmit and receive channels to measure differences in backscatter due to orientation, shape and material composition [R106][R107]. This leads ultimately to measurement of the 2x2 complex scattering matrix $\mathbf{S}$, from which we can synthesise the response of the image pixel to arbitrary polarisation combinations.

On the other hand, radar interferometry [R108] involves coherently combining signals from two separated spatial positions (defining the so called baseline of the interferometer) to extract a phase difference or interferogram. In radar this can be achieved in two main configurations, so called along-track interferometry, which involves time displacements between separated antennas along the flight direction of the platform leading to velocity estimation. Alternatively, we can perform across-track interferometry, involving lateral separation of antennas and leading to spatial information relating to the elevation of the scatterer above a reference ground position. In PolInSAR interest centre mainly on across-track geometries but in principle it can be applied to along track configurations as well.

PolInSAR differs from conventional interferometry in that it allows generation of interferograms for arbitrary transmit and receive polarisation pairs. It turns out that the phase of an interferogram changes with the choice of polarisation and consequently we can extract important biophysical and geophysical parameters by interpreting this change in the right way. It shall be seen that consequently the combination of interferometry with polarimetry is greater than the sum of its parts and that PolInSAR allows us to overcome severe limitations of both techniques when taken alone. This is especially true in the important area of remote sensing of vegetated land surface, where polarimetry suffers from the inherent high entropy problem [R106], while standard interferometry remains underdetermined, i.e., the interferogram depends on many possible physical effects, no one of which can be identified from the data itself [R109][R110].

1.2 SAR Interferometry

PolInSAR algorithms make use of interferometric coherence, or equivalently phase and local phase variance, rather than backscattered power [R111][R112][R113][R114]. For this reason it is necessary to introduce and to study the problems associated with the estimation of coherence from radar data, especially in the case of interferometric data. A similar introduction for polarimetric data was already seen in Section **Erreur ! Source du renvoi introuvable.**. Starting with any two co-registered single look complex (SLC) data channels S_1 and S_2 the interferometric coherence is formally defined as

$$\gamma = |\gamma| e^{i\phi} = \frac{E\{S_1 S_2^*\}}{\sqrt{E\{S_1 S_1^*\}}\sqrt{E\{S_2 S_2^*\}}} \tag{1.1}$$

where $0 \le |\gamma| \le 1$. In practice the sample coherence is frequently used as a coherence estimate of Eq. (1.1)

$$\delta = |\delta| e^{i\chi} = \frac{\sum_{k=1}^{n} S_{1k} S_{2k}^{*}}{\sqrt{\sum_{m=1}^{n} S_{1k} S_{1k}^{*}} \sqrt{\sum_{m=1}^{n} S_{2k} S_{2k}^{*}}} \tag{1.2}$$

where k is the sample number and we have only a finite number n independent signal measurements available. Eq. (1.2) represents the maximum likelihood (ML) estimate of coherence and under some general statistical assumptions provides an estimate that is asymptotically unbiased. For jointly complex Gaussian processes S_1 and S_2 the probability density function (pdf) of $|\delta|$ can then be derived as a function of the true coherence value $|\gamma|$ and the number of samples M [R69]

$$p\left(|\delta| \middle| |\gamma|\right) = 2(n-1)\left(1-|\gamma|^2\right)^n |\delta| \left(1-|\delta|^2\right)^{n-2} F\left(n, n; 1; |\delta|^2 |\gamma|^2\right) \tag{1.3}$$

where F is a special mathematical function called the hypergeometric function [R114]. More significant for Pol-InSAR is estimation of the bias in the coherence magnitude, derived from Eq. (1.3) as the first moment of $|\delta|$

$$E\{|\delta|\} = \frac{\Gamma(n)\Gamma\left(1+1/2\right)}{\Gamma\left(n+1/2\right)} {}_3F_2\left(3/2, n, n; n+1/2; 1; |\delta|^2\right)\left(1-|\delta|^2\right)^n \tag{1.4}$$

where ${}_pF_q$ is the generalized hypergeometric function. As it can be observed from the previous expression, the estimate is consistently biased towards higher values; in the extreme case of one–look estimation the coherence estimate is equal to unity and so always overestimated. However, the bias decreases with increasing number of independent samples n and with increasing underlying coherence $|\gamma|$.

A second important consequence of Eq. (1.3) is estimation of the variance of the sample coherence magnitude. This is required to assess the precision of parameters estimated from the coherence and impacts on the accuracy of derived products such as vegetation height. The most accurate way to estimate this variance is to consider $\mathrm{var}\{|\delta|\} = E\{|\delta|^2\} - E\{|\delta|\}^2$, where

$$E\{|\delta|^2\} = \frac{\Gamma(n)\Gamma(1+1)}{\Gamma(n+1)} {}_3F_2\left(2, n, n; n+1; 1; |\delta|^2\right)\left(1-|\delta|^2\right)^n \tag{1.5}$$

Employing the same procedure to obtain the distribution of the coherence magnitude, one my derive the distribution of the interferometric phase

$$p(\chi | \phi, |\gamma|) = \frac{\Gamma\left(n+1/2\right)\left(1-\gamma^2\right)^n \beta}{2\sqrt{\pi}\Gamma(n)\left(1-\beta^2\right)^{M+\frac{1}{2}}} + \frac{\left(1-|\gamma|^2\right)^n}{2\pi} F\left(n, 1; \frac{1}{2}; \beta^2\right) \quad \text{where} \quad \begin{cases} -\pi < \chi \le \pi \\ \beta = |\gamma| \cos(\chi - \phi) \end{cases} \tag{1.6}$$

which can be used to formally estimate the variance of the phase estimate as

$$\mathrm{var}\{\phi\} = \int_{-\pi}^{\pi} \chi^2 p(\chi|\phi,|\gamma|)\, d\chi \tag{1.7}$$

For a small number of looks, the hypergeometric functions can be replaced by simpler trigonometric functions [R115], but for $n > 4$, as generally required for PoLInSAR applications, the full calculation is required. While these equations provide the most accurate method of assessing bias and complex coherence variance, often we assume zero bias, by using sufficient averaging, and estimate the variance by making use of simpler equations for speedier computation. In particular, the Cramer-Rao bounds provide lower limits on the variance for coherence and phase and have been derived in [R116] to provide the simpler formulae

$$\mathrm{var}\{|\gamma|\} = \frac{\left(1-|\gamma|^2\right)^2}{2M} \le \mathrm{var}\{|\delta|\} \qquad \mathrm{var}\{\phi\} = \frac{1-|\gamma|^2}{2M|\gamma|^2} \le \mathrm{var}\{\chi\} \tag{1.8}$$

As it can be deduced for phase based processing, it is always better to operate at high coherence and avoid low coherences, the latter involving not only increased variance but also severe bias issues that can distort the phase information. It is a key limitation of polarimetry that scattering by vegetation leads to low coherences for all polarization channels because of so called depolarization. This severely limits the ability to use polarimetric phase information over vegetated land surfaces. Interferometry on the other hand allows to partially control coherence via baseline selection. PolInSAR exploits this advantage to obtain high coherence in multiple polarization channels.

The above considerations for coherence estimation are important in PolInSAR, the major distinguishing feature of which is that we add an extra stage in the construction of the two SLC channels S_1 and S_2. In general, for a fully polarimetric, or quadpol data set, we take as input the three calibrated SLC images S_{hh}, S_{hv} and S_{vv} and generate projections of these onto user defined *complex* weight vectors $\mathbf{w}_1$ and $\mathbf{w}_2$ before calculating the coherence defined as

$$\left.\begin{aligned} s_1 &= w_1^1 \frac{\left(S_{hh}^1 + S_{vv}^1\right)}{\sqrt{2}} + w_1^2 \frac{\left(S_{hh}^1 - S_{vv}^1\right)}{\sqrt{2}} + w_1^3 \sqrt{2} S_{hv}^1 = \mathbf{w}_1^T \cdot \mathbf{k}_1 \\ s_2 &= w_2^1 \frac{\left(S_{hh}^2 + S_{vv}^2\right)}{\sqrt{2}} + w_2^2 \frac{\left(S_{hh}^2 - S_{vv}^2\right)}{\sqrt{2}} + w_2^3 \sqrt{2} S_{hv}^2 = \mathbf{w}_2^T \cdot \mathbf{k}_2 \end{aligned}\right\}$$
$$\Rightarrow \gamma(\mathbf{w}_1, \mathbf{w}_2) = \frac{E\{S_1 S_2^*\}}{\sqrt{E\{S_1 S_1^*\}}\sqrt{E\{S_2 S_2^*\}}} \tag{1.9}$$

The weight vectors $\mathbf{w}_1$ and $\mathbf{w}_2$ define user selected scattering mechanisms at ends 1 and 2 of the across-track baseline. In general $\mathbf{w}_1$ and $\mathbf{w}_2$ can be different and both parameterised as complex unitary vectors of the form shown previously [R106][R95]. The weight vectors or scattering mechanisms in which the targets vectors could be projected could be the canonical mechanisms detailed previously. However, it is a feature of PolInSAR algorithm development that use is often made of more general $\mathbf{w}$ vectors than those shown, derived for example as eigenvectors for coherence optimisation [R94][R117][R118][R119][R120] or through a prior model studies of scattering from vegetated terrain [R121][R122]. For this reason we need to keep the more general notation so as to be able to consider arbitrary vectors in the formation of an interferogram. We now turn to consider such optimisation algorithms in more detail and to briefly assess their implications for coherence estimation and validation.

1.3 Algorithms for Optimum Interferogram Generation

Polarimetric Interferometry is a special case of multi-channel coherent radar processing [R123]. Such problems are characterised by multi-dimensional covariance matrices [R115][R124][R125]. In Polarimetric SAR for example, interest centres on the 3x3 hermitian coherency matrix $\mathbf{T}$, unitarily equivalent to the covariance matrix $\mathbf{C}$ as shown previously. This is the basic building block in polarimetric interferometry and so it can be designated as $\mathbf{\Lambda}_1$ to indicate how it relates to fully polarimetric measurements but made at only 1 spatial position. In single baseline PolInSAR a second measurement at a displaced position 2 is added. This is now characterised by a 6x6 coherency matrix $\mathbf{\Lambda}_2$ as shown in Eq. (1.10). The 6 x 6 matrix can be naturally partitioned into 3 sub matrices each of size 3x3. This formulation then scales in a natural way for multi-baseline PolInSAR by expansion of the governing coherency matrix $\mathbf{\Lambda}_N$ to a 3N x 3N complex system or 4N x 4N for bistatic multi-baseline PolInSAR

$$\mathbf{\Lambda}_1 = \mathbf{T} \rightarrow \mathbf{\Lambda}_2 = \begin{bmatrix} \mathbf{T}_{11} & \mathbf{\Omega}_{12} \\ \mathbf{\Omega}_{12}^H & \mathbf{T}_{22} \end{bmatrix} \rightarrow \mathbf{\Lambda}_N = \begin{bmatrix} \mathbf{T}_{11} & \mathbf{\Omega}_{12} & \cdots & \mathbf{\Omega}_{1N} \\ \mathbf{\Omega}_{12}^* & \mathbf{T}_{22} & \cdots & \mathbf{\Omega}_{2N} \\ \vdots & \vdots & \ddots & \vdots \\ \mathbf{\Omega}_{1N}^* & \mathbf{\Omega}_{2N}^* & \cdots & \mathbf{T}_{NN} \end{bmatrix} \tag{1.10}$$

Returning now to the important case of $\mathbf{\Lambda}_2$, two of the sub-matrices, $\mathbf{T}_{11}$ and $\mathbf{T}_{22}$ are Hermitian and relate to the polarimetry from positions 1 and 2 while the third $\mathbf{\Omega}_{12}$ is a complex 3x3 matrix that contains information about the variation of interferometric coherence and phase for all possible weight vectors $\mathbf{w}_1$ and $\mathbf{w}_2$

$$\gamma(\mathbf{w}_1, \mathbf{w}_2) = \frac{\mathbf{w}_1^H \mathbf{\Omega}_{12} \mathbf{w}_2}{\sqrt{\mathbf{w}_1^H \mathbf{T}_{11} \mathbf{w}_1} \cdot \sqrt{\mathbf{w}_2^H \mathbf{T}_{22} \mathbf{w}_2}} \tag{1.11}$$

The previous relation leads to an important choice of approach to algorithm development in PolInSAR. In the first case, if the vectors $\mathbf{w}_1$ and $\mathbf{w}_2$ are known in advance, then the coherence can be directly estimated using Eq. (1.9) with the same InSAR fluctuation statistics and bias outlined in the previous section. However, often we wish to determine *optimum* weight vectors from the data itself and it follows from Eq. (1.11) that to do this we require estimates of the three 3x3 matrices , $\mathbf{T}_{11}$ and $\mathbf{T}_{22}$ and $\mathbf{\Omega}_{12}$. This opens up a much wider discussion about the fluctuation statistics and bias arising from the fact that only estimates and not true matrix values can be used in Eq. (1.11). For example, to estimate the submatrices we must first estimate the full 6x6 coherency matrix $\mathbf{\Lambda}_2$. This estimate $\mathbf{Z}$ is obtained by means of the multilook estimator given previously.

One important application of Eq. (1.11) is the calculation of the optimum coherences in PolInSAR. The most general formulation of this was first presented in [R94][R95] and is summarised in Eq. (1.12). Here, we first state the problem mathematically, which is to choose $\mathbf{w}_1$ and $\mathbf{w}_2$ so as to maximise the coherence magnitude, defined from the complex coherence as a function of the three sub-matrices $\mathbf{T}_{11}$ and $\mathbf{T}_{22}$ and $\mathbf{\Omega}_{12}$ as shown. This can be mathematically solved by using a Lagrange multiplier technique as shown and leads to the calculation of the required $\mathbf{w}$ vectors as eigenvectors of a pair of matrices, themselves defined as products of the composite matrices

$$\max_{\mathbf{w}_1,\mathbf{w}_2} \frac{\mathbf{w}_1^H \boldsymbol{\Omega}_{12} \mathbf{w}_2}{\sqrt{\mathbf{w}_1^H \mathbf{T}_{11} \mathbf{w}_1} \cdot \sqrt{\mathbf{w}_2^H \mathbf{T}_{22} \mathbf{w}_2}}$$

$$L = \mathbf{w}_1^H \boldsymbol{\Omega}_{12} \mathbf{w}_2 + \lambda_1 \left(\mathbf{w}_1^H \mathbf{T}_{11} \mathbf{w}_1 - 1 \right) + \lambda_2 \left(\mathbf{w}_2^H T_{22} \mathbf{w}_2 - 1 \right)$$

$$\Rightarrow \begin{cases} \dfrac{\partial L}{\partial \mathbf{w}_1^H} = \boldsymbol{\Omega}_{12} \mathbf{w}_2 + \lambda_1 \mathbf{T}_{11} \mathbf{w}_1 = 0 \\ \dfrac{\partial L}{\partial \mathbf{w}_2^H} = \boldsymbol{\Omega}_{12}^{*T} \mathbf{w}_1 + \lambda_2 T_{22} \mathbf{w}_2 = 0 \end{cases} \tag{1.12}$$

$$\Rightarrow \begin{cases} \mathbf{T}_{22}^{-1} \boldsymbol{\Omega}_{12}^H \mathbf{T}_{11}^{-1} \boldsymbol{\Omega}_{12} \mathbf{w}_2 = \lambda_1 \lambda_2^* \mathbf{w}_2 \\ \mathbf{T}_{11}^{-1} \boldsymbol{\Omega}_{12} \mathbf{T}_{22}^{-1} \boldsymbol{\Omega}_{12}^H \mathbf{w}_1 = \lambda_1 \lambda_2^* \mathbf{w}_1 \end{cases}$$

As it was noted in Section 1.2, the coherence magnitude estimated value is biased respect to the true value in such a way that the larger the number of averaged samples and the higher the coherence magnitude, the lower the bias. The previous hypothesis was based on considering Eq. (1.9) where the vectors $\mathbf{w}_1$ and $\mathbf{w}_2$ are known in advance. Nevertheless, if Eq. (1.12) is considered to obtain the coherence magnitude, the vectors $\mathbf{w}_1$ and $\mathbf{w}_2$ must also be estimated from the data, leading to a larger coherence magnitude bias.

In order to obtain an optimization approach that has less bias for a given number of samples, it is necessary to reduce the effective dimensionality of the problem. Several authors have proposed adopting the a prior assumption $\mathbf{w}_1 = \mathbf{w}_2$, i.e., that the optimum coherence vector remains unknown but we assume that it doesn't change with baseline [R126][R127][R128][R129][R119][R120]. This idea is supported on physical grounds for short baselines in the absence of temporal decorrelation, i.e., for single pass or low frequency sensors where the scattering does not change significantly over the effective angular width of the baseline. This approach calls for a new mathematical formulation of the optimization process. One approach is based on a straightforward extension of the Lagrange multiplier technique to constrain $\mathbf{w}_1 = \mathbf{w}_2$ [R120]. This leads by manipulation of Eq. (1.12) to a set of $\mathbf{w}$ vectors given as eigenvectors of the composite matrix

$$\left(\mathbf{T}_{11} + \mathbf{T}_{22} \right)^{-1} \left(\boldsymbol{\Omega}_{12} + \boldsymbol{\Omega}_{12}^H \right) \mathbf{w} = -\lambda \mathbf{w} \tag{1.13}$$

One problem with the previous equation is that the eigenvalue is not the coherence, but its real part and so the optimization is phase sensitive. For this reason, a second related approach based on maximization of the phase difference as a function of polarization vector $\mathbf{w}$ has been developed. In this case, the optimum vector is found by solving a phase parameterised eigenvalue problem [R128][R119]

$$\boldsymbol{\Omega}_H \mathbf{w} = \lambda \mathbf{T} \mathbf{w} \quad \begin{cases} \boldsymbol{\Omega}_H = \dfrac{1}{2} \left(\boldsymbol{\Omega}_{12} e^{i\phi_1} + \boldsymbol{\Omega}_{12}^H e^{-i\phi_1} \right) \\ \mathbf{T} = \dfrac{1}{2} \left(\mathbf{T}_{11} + \mathbf{T}_{22} \right) \end{cases} \tag{1.14}$$

This has been shown to be equivalent to calculating the numerical radius of the complex matrix $\mathbf{A} = \mathbf{T}^{-1/2} \boldsymbol{\Omega}_{12} \mathbf{T}^{-1/2}$. A proposed algorithm for finding this optimum state has been presented in [R119][R130]. One drawback in this approach is that ϕ_1 is a free parameter and so either search or iterative methods must be used to secure the global optimum. This adds to the computational complexity for each pixel.

A third related approach has been proposed based on a sub-space Monte Carlo searching algorithm [R126][R127]. This limits the search for the optimum (again assuming $\mathbf{w}_1 = \mathbf{w}_2$) to the diagonal elements of $\boldsymbol{\Omega}_{12}$, i.e., to copolarised or

crosspolarised combinations across the whole Poincaré sphere. This again acts to effectively limit the dimensionality of the problem and demonstrates less bias than the full Lagrange multiplier method. Finally, phase centre super-resolution techniques based on the ESPRIT algorithm have also been proposed to find the optimum $\mathbf{w}$ vectors [R131].

In all these cases a sub-optimum solution is obtained compared to the unconstrained Lagrange multiplier method but often with better numerical stability. Given the general increased processing overhead of employing optimization, it is always of interest to investigate the potential benefits of employing an optimization approach over simple linear, Pauli and circular options.

1.4 Model Based Polarimetric SAR Interferometry

The previous section considered an important optimisation problem in PolInSAR, namely to investigate the maximum variation of coherence with polarisation by solving an eigenvalue problem. This section will be focused on some canonical problems of interest in the remote sensing of land surfaces and try and use the mathematical solutions obtained to conclude as to the potential of optimisation versus standard coherence estimation in PolInSAR. We consider three important problems, scattering from non-vegetated surfaces, random volume scattering and finally a 2-layer surface+volume mixture which more closely matches the behaviour of natural vegetated land surfaces.

1.4.1 PolInSAR for Bare Surface Scattering

The starting point will be to consider the simplest case of non-vegetated terrain. Under the assumption of surface scattering only, the polarimetry can then be characterised as a reflection symmetric random media with a coherency matrix $\mathbf{T}$ of the form shown in Eq. (1.15) [R106][R132]. The interferometry, following range spectral filtering [Gatelli 1994] and assuming no temporal or SNR decorrelation, is characterised by a single parameter, the ground phase ϕ

$$\begin{aligned}\mathbf{K} &= \mathbf{T}_{11}^{-1}\boldsymbol{\Omega}_{12}\mathbf{T}_{11}^{-1}\boldsymbol{\Omega}_{12}^{H} \\ &= \begin{bmatrix} t_{11} & t_{12} & 0 \\ t_{12}^{*} & t_{22} & 0 \\ 0 & 0 & t_{33} \end{bmatrix}^{-1} e^{i\phi} \begin{bmatrix} t_{11} & t_{12} & 0 \\ t_{12}^{*} & t_{22} & 0 \\ 0 & 0 & t_{33} \end{bmatrix} \begin{bmatrix} t_{11} & t_{12} & 0 \\ t_{12}^{*} & t_{22} & 0 \\ 0 & 0 & t_{33} \end{bmatrix}^{-1} e^{-i\phi} \begin{bmatrix} t_{11} & t_{12} & 0 \\ t_{12}^{*} & t_{22} & 0 \\ 0 & 0 & t_{33} \end{bmatrix} = \begin{bmatrix} 1 & 0 & 0 \\ 0 & 1 & 0 \\ 0 & 0 & 1 \end{bmatrix}\end{aligned} \qquad (1.15)$$

From the previous equation it follows that the optimum coherences are obtained as eigenvectors of the matrix $\mathbf{K}$ as shown. By multiplying terms we see that the matrix $\mathbf{K}$ is just the 3x3 identity matrix. This implies that all polarisations have the same interferometric coherence and POLInSAR plays no role in surface scattering problems. This is not quite true in practice for two important reasons: in practice there will be polarisation dependent SNR decorrelation. In fact, recently it has been suggested that such SNR coherence variations with polarimetry be used for quantitative InSAR surface parameter estimation. This formulation assumes that the scattering from the surface occurs within a thin layer. If there is significant penetration into the surface, then volume scattering effects can occur and this will lead to volume decorrelation effects. These effects have been observed for land ice [R103] and snow studies [R104] where the surface is non-vegetated but covered by a low loss scattering layer. Nonetheless, Eq. (1.15) demonstrates how for bare surface scattering PolInSAR plays only a secondary role. More interesting for application of natural land surfaces is to consider the presence of volume scattering due to vegetation cover.

1.4.2 Pol-InSAR for Random Volume Scattering

When considering scattering from a volume, interest centres on the special case of a random volume, i.e., one with macroscopic azimuthal symmetry [R106]. In this case the polarimetric coherency matrix $\mathbf{T}$ is diagonal. However, more care is required over consideration of the interferometric phase in $\boldsymbol{\Omega}_{12}$. In this case one must include the effects

of volume decorrelation due to the random vertical distribution of scatterers [Treuhaft 1996,2000, Cloude 2003]. In this case, the interferometry must include a complex integral I_2 normalised by a real integral I_1.

$$\begin{aligned}\mathbf{K} &= \mathbf{T}_{11}^{-1}\boldsymbol{\Omega}_{12}\mathbf{T}_{11}^{-1}\boldsymbol{\Omega}_{12}^{H} \\ &= \frac{1}{I_1}\begin{bmatrix}\frac{1}{t_{11}} & 0 & 0\\ 0 & \frac{1}{t_{22}} & 0\\ 0 & 0 & \frac{1}{t_{33}}\end{bmatrix} I_2 \begin{bmatrix}t_{11} & 0 & 0\\ 0 & t_{22} & 0\\ 0 & 0 & t_{33}\end{bmatrix} \frac{1}{I_1}\begin{bmatrix}\frac{1}{t_{11}} & 0 & 0\\ 0 & \frac{1}{t_{22}} & 0\\ 0 & 0 & \frac{1}{t_{33}}\end{bmatrix} I_2^{*} \begin{bmatrix}t_{11} & 0 & 0\\ 0 & t_{22} & 0\\ 0 & 0 & t_{33}\end{bmatrix} \\ &= \left|\frac{I_2}{I_1}\right|^2 \begin{bmatrix}1 & 0 & 0\\ 0 & 1 & 0\\ 0 & 0 & 1\end{bmatrix}\end{aligned} \tag{1.16}$$

where

$$\begin{aligned} I_1 &= e^{-\frac{2\sigma h_v}{\cos\theta_o}} \int_0^{h_v} e^{\frac{2\sigma z'}{\cos\theta_o}} dz' \\ I_2 &= e^{-\frac{2\sigma h_v}{\cos\theta_o}} \int_0^{h_v} e^{\frac{2\sigma z'}{\cos\theta_o}} e^{ik_z z'} dz' \end{aligned} \tag{1.17}$$

where the vegetation is characterized by a height h_v and mean extinction rate σ and θ_0 represents the mean incidence angle. In Eq. (1.16), it is also observed that $\mathbf{K}$ is proportional to the identity matrix, but this time the eigenvalues, all equal, are given by a ratio of integrals over the vertical distribution. This ratio is just the volume decorrelation displaying an increase in phase variance and a vegetation bias to the ground phase determined by h_v and σ

$$\begin{aligned}\gamma(\mathbf{w}) &= \frac{I_2}{I_1} = \frac{2\sigma\, e^{i\phi(z_o)}}{\cos\theta_o (e^{2\sigma\, h_v/\cos\theta_o} - 1)} \int_0^{h_v} e^{ik_z z'} e^{\frac{2\sigma\, z'}{\cos\theta_o}} dz' \\ &= \frac{p}{p_1}\frac{e^{p_1 h_v} - 1}{e^{p h_v} - 1} = \gamma_v\end{aligned} \tag{1.18}$$

where

$$\begin{aligned} p &= \frac{2\sigma}{\cos\theta_0} \\ p_1 &= p + ik_z \\ k_z &= \frac{4\pi\Delta\theta}{\lambda \sin\theta_0} \approx \frac{4\pi B_n}{\lambda H \tan\theta_0} \end{aligned} \tag{1.19}$$

Here the vertical interferometric wavenumber k_z [R108] appears as a function of the normal baseline B_n, the wavelength λ ,as well as the sensor height H. $\Delta\theta$ is the angular separation of the baseline end points from the surface pixel.

As it can be observed in (1.18), this coherence is independent of polarisation, $\mathbf{K}$ has 3 degenerate eigenvalues and PolInSAR plays no role in the analysis of random volume scattering. This statement has to be modified in the presence of oriented volumes [R133][R134], i.e., ones with a preferred orientation of scattering elements such as occur in some agricultural crops and even in forestry applications at low frequencies [R134]. In such cases PolInSAR does indeed play a role for volume scattering, with $\mathbf{K}$ developing 3 distinct eigenvalues. However, for the treatment of forestry applications at L-band and above, such orientation effects are small and the random volume assumption is justified [R135][R136].

In conclusion, both bare surfaces and random volumes lead to a degenerate eigenvalue spectrum for the matrix $\mathbf{K}$. It is only when we combine these two effects together that we start to see the potential benefits of employing PolInSAR processing.

1.4.3 PolInSAR 2-Layer Combined Surface and Random Volume Scattering

In the general case when combined surface and volume scattering occurs then PolInSAR coherence optimisation becomes useful as it is now demonstrated. In this 2-layer case or Random-Volume-over-Ground (RVoG) model approach [R110][R137], the observed coherence is given by a mixture formula

$$\gamma(\mathbf{w}) = e^{i\phi}\frac{\tilde{\gamma}_v + \mu(\mathbf{w})}{1+\mu(\mathbf{w})} = e^{i\phi}\left[\gamma_v + \frac{\mu(\mathbf{w})}{1+\mu(\mathbf{w})}(1-\gamma_v)\right] \tag{1.20}$$

Here, the ground phase ϕ and complex volume coherence γ_v are combined with a new real parameter μ , the ratio of effective surface, i.e., all scattering contributions with a phase centre located at ϕ, to volume scattering. In effect when $\mu = 0$, the scattering reduces to the case of random volume scattering while when μ tends to infinity it reduces to the surface scattering case. Interest centres on the intermediate case because one has an unknown but constant complex number contribution from the volume scattering combined with a polarisation dependent surface term. By isolating the polarisation dependent terms the resulting coherence then lies along a straight line in the complex coherence plane as shown in (1.20).

This straight line model has been successfully tested on varied forest data sets [Isola 2001, Papathanassiou 2001, 2005] and seems to be a good fit for L- and P-band PolInSAR forestry applications. It is interesting to note how the coherence varies as we adjust the single parameter μ along this line. Figure 1.1 illustrates three important cases. In all three we first note how the coherence starts for small μ at some value depending on the volume scattering contribution, 0.8 in the example. It then initially decreases with increasing surface contribution until reaching a turning point after which it increases with μ , always approaching unity as μ tends to infinity.

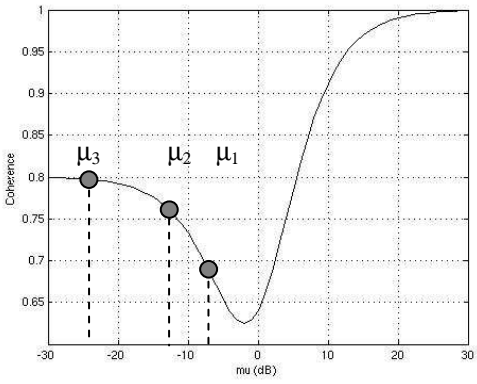

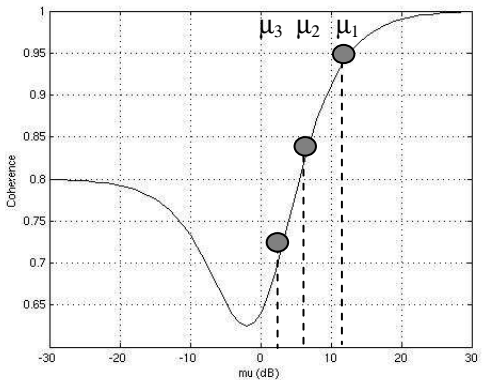

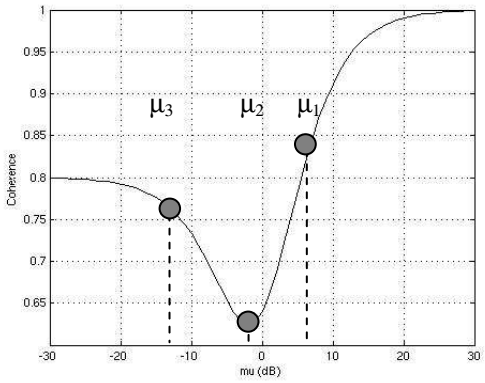

Figure 1.1 – Variation of Coherence with small (top left), large (top right) and intermediate (lower) μ values.

In Figure 1.1 three important special cases of the eigenvalue spectrum of $\mathbf{K}$ for this scenario are also superimposed. The top-left shows the case when μ is always small, i.e., when there is strong volume scattering with high extinction masking the surface contributions. As polarisation $\mathbf{w}$ is adjusted, then μ will also change and the optimiser has an incentive to select the *minimum* μ channel to *maximise* coherence. At the other extreme, when μ is large and surface scattering dominates, we see that the optimiser has an incentive instead to *maximise* μ in order to *maximise* coherence. A more interesting case, and one that occurs often in practice for L-band forestry applications, is the intermediate zone when the variation of μ (the μ spectrum) includes the turning point. In this case the coherence can be maximised by either increasing or decreasing μ depending on circumstances.

Two important conclusions can be made from this, firstly that in the mixed surface plus volume scattering case, the coherence varies with polarisation and so optimisation plays a role in PolInSAR analysis. Secondly we see that we cannot simply associate the maximum coherence with for example the maximum value of μ. Both maxima and minima of μ can lead to the optimum coherence, depending on the circumstances. However, it follows that if we can estimate the μ spectrum for any problem then we can compare the max/min with the values for the standard channel (linear, Pauli etc) to quantify the potential benefits of employing optimisation techniques.

The determination of the extreme points of the μ spectrum is related to a classical problem in radar polarimetry, namely contrast optimisation [R138]. The solution to this is obtained as the eigenvalues of the product of the inverse volume times the surface polarimetric coherency matrices

$$\left.\begin{aligned} \mathbf{T}_V = mI_1\begin{bmatrix}1&0&0\\0&\kappa&0\\0&0&\kappa\end{bmatrix} \Rightarrow \mathbf{T}_v^{-1} = \frac{1}{mI_1}\begin{bmatrix}1&0&0\\0&\frac{1}{\kappa}&0\\0&0&\frac{1}{\kappa}\end{bmatrix} \\ \mathbf{T}_s = \begin{bmatrix}t_{11}&t_{12}&0\\t_{12}^*&t_{22}&0\\0&0&t_{33}\end{bmatrix} \end{aligned}\right\} \Rightarrow \mathbf{T}_v^{-1}\mathbf{T}_s = \frac{1}{I_1 m}\begin{bmatrix}t_{11}&t_{12}&0\\\frac{t_{12}^*}{\kappa}&\frac{t_{22}}{\kappa}&0\\0&0&\frac{t_{33}}{\kappa}\end{bmatrix} \quad (1.21)$$

Under the assumption of a random volume and reflection symmetric surface scattering component, the eigenvalues of this matrix can be determined analytically as

$$\begin{cases} \mu_1 = \dfrac{1}{2I_1 m}\left(t_{11} + \dfrac{t_{22}}{\kappa} + \sqrt{\left(t_{11} - \dfrac{t_{22}}{\kappa} \right)^2 + \dfrac{4\left|t_{12}\right|^2}{\kappa}} \right) \\ \mu_2 = \dfrac{1}{2I_1 m}\left(t_{11} + \dfrac{t_{22}}{\kappa} - \sqrt{\left(t_{11} - \dfrac{t_{22}}{\kappa} \right)^2 + \dfrac{4\left|t_{12}\right|^2}{\kappa}} \right) \\ \mu_3 = \dfrac{1}{I_1 m}\left(\dfrac{t_{33}}{\kappa} \right) \end{cases} \Rightarrow \begin{cases} \left|\gamma_1\right| e^{i\delta_1} = \dfrac{e^{i\phi_0}(\gamma_v + \mu_1)}{1+\mu_1} \\ \left|\gamma_2\right| e^{i\delta_2} = \dfrac{e^{i\phi_0}(\gamma_v + \mu_2)}{1+\mu_2} \\ \left|\gamma_3\right| e^{i\delta_3} = \dfrac{e^{i\phi_0}(\gamma_v + \mu_3)}{1+\mu_3} \end{cases} \quad (1.22)$$

Equally importantly, the eigenvectors of this matrix indicate the $\mathbf{w}$ vectors that should be employed in PolInSAR to secure these extreme coherence values. We note from Eq. (1.22) that the optimum contrast solutions are not generally the simple HH, HV and VV channels and this supports investigation of optimisation techniques based fully polarimetric data acquisition for Pol-InSAR processing.

2 Polarimetric SAR Tomography (Pol-TomSAR)

2.1 Introduction

3-D SAR Tomography (SARtom) is an experimental multibaseline (MB) interferometric mode achieving full 3-D imaging in the range-azimuth-height space through elevation beam forming, i.e. spatial (baseline) spectral estimation [R139][R140]. Thanks to SARtom, the resolution of multiple scatterers is made possible in height in the same range-azimuth cell, overcoming a limitation of the conventional InSAR processing and complementing PolInSAR. SARTom can add more features for the analysis of complex scenarios, e.g. for the estimation of forest height and biomass, sub-canopy topography, soil humidity and ice thickness monitoring, and extraction of heights and reflectivities in layover urban areas [R139][R141]. In order to retrieve information on the nature of the imaged scatterers, SARtom has also been extended to include the polarimetric information (briefly, Pol-TomSAR) [R142]. It jointly exploits MB SAR data acquired with different polarization channels to improve the accuracy of the estimation of the vertical position of the imaged scatterers, and to estimate a set of normalized complex coefficients characterizing the corresponding polarimetric scattering mechanism.

The very first demonstration of the tomographic concept was carried out in 1995 by processing single-polarization data acquired in an anechoic chamber of a two-layer synthetic target [R143]. SARtom was then experimented from an airborne platform a few years later by acquiring L-band data by means of the DLR E-SAR platform over the Oberpfaffenhofen site [R139]. Although this experiment was successful in demonstrating the 3-D imaging capabilities of forest volumes and man-made targets at L-band, two main limitations of SARtom were apparent, namely the usually low number of images available for processing to avoid large acquisition times and the consequent temporal decorrelation, and the difficulty of obtaining ideal planned uniformly spaced parallel flight tracks due to navigation/orbital considerations.

In order to mitigate the effects of acquisition non-idealities, most of the subsequent research on (single polarization) SARTom investigated different imaging solutions, model-based and not [R140][R147]. Many experiments have shown that the use of polarimetric information not only increments the number of observables, but it also allows to enhance the accuracy of height estimation of scatterers, increase height resolution, and to estimate a vector of complex coefficients describing the scattering mechanism at each height [R142], [R148][R153]. In forest scenarios, the combination of multi-baseline polarimetric data can be used to separate ground and canopy scattering, and to estimate their vertical structures by following a relatively simple algebraic approach [R146].

2.2 SARtom and Pol-TomSAR as Spectral Estimation Problems

2.2.1 Non-model Based Adaptive Solutions

As usual in SAR imaging and interferometry, after focusing in the range-azimuth plane, the K SAR images available for processing are assumed to be co-registered and properly compensated for the flat-Earth phase. Moreover, N independent looks (here multiple adjacent pixels) are used for processing. For each n-th look, the complex amplitudes of the pixels observed in the K SAR images at the same range-azimuth coordinate are collected in the $K\times 1$ complex-valued vector $\mathbf{y}(n)$ [R140]-[R141]. $\mathbf{y}(n)$ it is characterized by its covariance matrix $\mathbf{R}=E\{\mathbf{y}^H\mathbf{y}\}$, where $E\{\cdot\}$ and denotes the statistical expectation. It can be demonstrated that the generic (l,m)-th element of $\mathbf{R}$ can be written as:

$$[\mathbf{R}]_{l,m}=\int P(z)\exp\{j(k_{z,l}-k_{z,m})z\}dz \tag{2.1}$$

where $P(z)$ is the wanted vertical distribution of the backscattered power (from here on, the tomogram) as a function of the height z and $k_{z,m}$ is the vertical wavenumber at the m-th baseline. From (2.1), it is apparent the Fourier relationship existing between the MB covariances and the tomogram, and it justifies the use of spectral estimation as a processing tool to estimate $P(z)$.

The inversion of (2.1) cannot be carried out through a plain Fourier-based 3-D focusing as it suffers from inflated sidelobes and poor height resolution. Among the investigated alternatives, a solution which has become a standard as a matter of fact is the adaptive beam forming (shortly, ABF), which is based on the Capon spectral estimator, and it has been demonstrated to have remarkable sidelobe rejection and resolution capabilities.

The single polarization ABF spectral estimation problem can be equivalently stated as the problem of designing a complex-valued finite impulse response filter $\mathbf{h}$ of order K that leaves undistorted the MB signal component at the height under test, say z, while rejecting possible other components from noise and other heights [R140]-[R141]. In formulas:

$$\min_{\mathbf{h}}\ \mathbf{h}^H\hat{\mathbf{R}}\mathbf{h}\ \text{subject to}\ \ \mathbf{h}^H\mathbf{a}(z)=1 \tag{2.2}$$

where $\mathbf{a}(z)$ is the so-called steering vector, with generic element $[\mathbf{a}(z)]_k=\exp\{jk_{z,k}z\}$ for $k=1,\ldots,K$, and $\hat{\mathbf{R}}$ is the sample covariance estimate. Notice that the resulting ABF filter $\mathbf{h}$ depends on $\hat{\mathbf{R}}$, and it varies with z; from this behaviour, the attribute 'adaptive'. In particular, the dependency on $\hat{\mathbf{R}}$ results into a null-placing at proper heights in the filtering operation, thus increasing resolution and sidelobe suppression in the final estimate of $P(z)$. The solution to the optimization problem (2.2) can be found in closed-form [R141].

If fully polarimetric data are available, without losing generality they can be combined in the Pauli basis. The resulting MB data vectors $\mathbf{y}_1(n)$, $\mathbf{y}_2(n)$ and $\mathbf{y}_3(n)$ can then be stacked one on top of the other in order to form the $3K$-dimensional MB-polarimetric data vector $\mathbf{y}_P(n)$. As a consequence, a MB-polarimetric sample covariance matrix $\hat{\mathbf{R}}_P$ can be calculated from $\mathbf{y}_P(n)$. Differently from the single polarimetric case, the tomogram has now to be estimated also by considering the polarization state at the targeted height. In this sense, the definition of the steering vector can be extended to the polarimetric case by means of a 3-dimensional target vector $\mathbf{k}$ whose elements are complex-valued coefficients describing the scattering mechanism in the Pauli basis, with $\|\mathbf{k}\|^2=1$. In formulas, the polarimetric steering vector $\mathbf{b}(z,\mathbf{k})$ is given by:

$$\mathbf{b}(z,\mathbf{k}) = \mathbf{B}(z)\ \mathbf{k} \tag{2.3}$$

where

$$\mathbf{B}(z) = \begin{bmatrix} \mathbf{a}(z) & \mathbf{0} & \mathbf{0} \\ \mathbf{0} & \mathbf{a}(z) & \mathbf{0} \\ \mathbf{0} & \mathbf{0} & \mathbf{a}(z) \end{bmatrix} \tag{2.4}$$

The ABF optimization problem (2.2) can be extended to the MB-polarimetric case as follows [R150]:

$$\min_{\mathbf{h}_P} \mathbf{h}_P^H \hat{\mathbf{R}}_P \mathbf{h}_P \text{ subject to } \mathbf{h}_P \mathbf{b}(z,\mathbf{k}) = 1 \tag{2.5}$$

where $\mathbf{h}_P$ is the MB-polarimetric ABF filter response. Now, $\mathbf{h}_P$ is optimized in order to place proper nulls in height and in the polarimetric space generated by $\mathbf{k}$. Notice that the dependence of $\mathbf{k}$ on z has been formally dropped for easiness of notation. From (2.5), the power of the filtered signal is:

$$\hat{P}_{ABF}(z,\mathbf{k}) = \frac{1}{\mathbf{b}^H(z,\mathbf{k})\ \hat{\mathbf{R}}_P\ \mathbf{b}(z,\mathbf{k})} \tag{2.6}$$

which is still a function of $\mathbf{k}$. To estimate the vertical power distribution as a function of the only z, and the corresponding $\mathbf{k}$, one can maximise (2.6) over $\mathbf{k}$ to finally obtain:

$$\hat{P}_{ABF}(z) = \frac{1}{\lambda_{\min}\left\{\mathbf{B}^H(z)\ \hat{\mathbf{R}}_P^{-1}\ \mathbf{B}(z)\right\}} \tag{2.7}$$

where $\lambda_{\min}\{\cdot\}$ denotes the minimum eigenvalue operator. The resulting $\hat{\mathbf{k}}_{ABF}(z)$ is the eigenvector associated to $\lambda_{\min}$. It is worth noting that the MB-polarimetric ABF estimator (2.7) is aimed to enhance the discrimination of particular scatterers or features. In other words, it is able to extract a rank-1 polarimetric information. This is generally the case of man-made targets like buildings in urban scenarios.

However, it can happen that the scatterers present at a given z are characterized by a random polarimetric behaviour, and they are more properly described by a 3×3 polarimetric covariance matrix $\mathbf{T}(z)$ rather than by a deterministic target vector [R151][R152]. This is generally the case in natural scenarios like forests. In this way, a scattering mechanism at the generic z will contribute to $\mathbf{R}_P$ with $\mathbf{T}(z)\otimes\left[\mathbf{a}(z)\mathbf{a}^H(z)\right]$, in which "$\otimes$" denotes the Kronecker product. In light of this, the polarimetric ABF estimator from the rank-1 formulation (2.7) can be extended in a full-rank sense [R152]. The derivation of such estimate is based on the definition of a full-rank objective function which uses the polarimetric span instead of the intensity associated to a given scattering mechanism. The full-rank ABF estimators then are:

$$\hat{P}_{ABF-FR}(z) = tr\left\{\left[\ \mathbf{B}^H(z)\ \hat{\mathbf{R}}_P^{-1}\mathbf{B}(z)\ \right]^{-1}\right\} \tag{2.8}$$

$$\hat{\mathbf{T}}_{ABF}(z) = \left[\ \mathbf{B}^H(z)\ \hat{\mathbf{R}}_P^{-1}\mathbf{B}(z)\ \right]^{-1} \tag{2.9}$$

The availability of the polarimetric coherence matrix makes possible the full exploitation of the polarimetric information for the characterization of the scattering, allowing the 3-D calculation of parameters like e.g. entropy and degree of polarization, as well as the application of polarimetric decompositions.

2.2.2 Model-based Pol-TomSAR

As mentioned in Section 1.6.1, the non-model based ABF possess some intrinsic degree of super-resolution, i.e. it is able to separate scatterers with a height difference lower than the Rayleigh resolution limit, which in turn depends on the maximum available baseline separation. However, a higher super-resolution could be needed in some applications. For this reason, a solution is to resort to model-based tomographic processors, which generally exploit the statistical description of the received signal or equivalently of the scattering behaviours present in the observed scene.

Several methods have been proposed for single- and then extended to full-polarization MB data sets. For instance, the MUSIC (multiple signal classification) is matched to point-like targets [R141], and it exploits the fact that the MB response of each point-like scatterer (i.e. the steering vector) in the backscattered radiation is orthogonal to the noise subspace. As a consequence, closed-form solution of the MUSIC PolSARtom functional can be found that outputs the scattering mechanism of each scatterer [R150][R151]. Still in the category of the eigen-based processors, the weighted signal subspace fitting can cope with more complex statistical descriptions of distributed and coherent scatterers (see [R151] for more details), although a multidimensional optimization is required.

Alternatively to the eigen-based PolSARtom, a solution that it is adaptive to both coherent and distributed scatterers, but possibly leading to a lower computational time, is the so-called covariance matching estimator (COMET). If the MB data are jointly Gaussian distributed, the knowledge of the MB-multipolarimetric covariance matrix $\mathbf{R}_P$ is enough to obtain a maximum likelihood (ML) estimation of the parameters describing the vertical distribution of the backscattered power. It can be demonstrated that the global ML problem can be decomposed by means of the extended invariance principle into a cascade of two ML problems (i.e. the estimation of $\mathbf{R}_P$ and the estimation of the parameters of interest from $\hat{\mathbf{R}}_P$), leading to an asymptotically equivalent solution and with a non-negligible reduction of the computational complexity. Under the Gaussian hypothesis, the resulting COMET estimates can be obtained from the following minimization problem:

$$\hat{\boldsymbol{\rho}} = \arg\min_{\boldsymbol{\rho}} \; tr\left\{\hat{\mathbf{R}}_P^{-1}\left[\mathbf{R}_P(\boldsymbol{\rho}) - \hat{\mathbf{R}}_P\right]\hat{\mathbf{R}}_P^{-1}\left[\mathbf{R}_P(\boldsymbol{\rho}) - \hat{\mathbf{R}}_P\right]\right\}, \tag{2.10}$$

where $\boldsymbol{\rho}$ is the vector containing the parameters to estimate. Equation (2.10) can be seen as the weighted Frobenius norm of the approximation error $\mathbf{R}_P(\boldsymbol{\rho}) - \hat{\mathbf{R}}_P$ with weight $\hat{\mathbf{R}}_P^{-1}$. Worth of notice, the COMET estimator can be used also when data are not Gaussian, although it is not asymptotically optimal anymore. COMET has been applied for the 3-D analysis of forest scenarios [R147], and it has been seen to convey estimates with satisfactory accuracy.

2.3 Coherence Tomography

Beside the development of "classical" tomography, also the so-called coherence tomography methods have been proposed which reconstruct the vertical distribution of scatterers from complex coherence measurements of volumetric scatterers like forests. In a few words, the structure function is approximated through a weighted sum of a series of basis functions [R144]. The individual parameterization has then to be inverted using a (limited) number of interferometric measurements at the same or different polarizations. In this class of algorithms, the different polarization channels can be used to find a polarization state with lowest ground contribution. Already operating with a dual baseline acquisition, such methods have been demonstrated to reconstruct reliably the vegetation vertical structure and to improve biomass estimation by combining forest height and vertical structure [R148]. The coherence tomography-based inversion is particularly attractive in view of single pass (polarimetric) interferometric mission (e.g. the DLR's Tandem-L proposal), where an interferometric coherence is available at each pass of the interferometer without relative phase difference and problems of temporal decorrelation.